Factors Influencing the Texture and Stability of Maghemite Obtained from the Thermal Decomposition of Lepidocrocite

G. S. Chopra,[†] C. Real,[†] M. D. Alcalá,[†] L. A. Pérez-Maqueda,[†] J. Subrt,[‡] and J. M. Criado*,[†]

Instituto de Ciencia de Materiales, Centro Mixto Universidad de Sevilla-C.S.I.C., c/Américo Vespucio s/n; Isla de La Cartuja, 41092 Sevilla, Spain, and Institute of Inorganic Chemistry, 25068 Rez, Czech Republic

Received November 12, 1998. Revised Manuscript Received February 4, 1999

The thermal decomposition of a series of lepidocrocite samples has been monitored by means of the Constant Rate Thermal Analysis (CRTA). This method allows controlling the reaction temperature in such a way that both the reaction rate and the partial pressure of the water vapor generated in the reaction are maintained constant at values that can be arbitrarily selected by the user. The final products obtained from the thermal dehydroxylation of the lepidocrocite precursors under residual pressures of water vapor ranging from 5×10^{-5} mbar to 10 mbar have been characterized by TEM, XRD, and Mösbauer spectroscopy. It has been concluded that they preserve the shape and size of the corresponding precursors. The precise control of the partial pressure of the water vapor self-generated in the above reaction allows tailoring the internal porosity of the maghemite−hematite mixture obtained as final product. It has been shown that the larger the particle size of the starting lepidocrocite is, the larger the porosity of the iron oxide obtained. The ratio γ-Fe_2O_3/α-Fe_2O_3 is strongly dependent on both the texture of the starting lepidocrocite and the partial pressure of water vapor selected for performing its dehydration. Thus, the percentage of maghemite increases by decreasing the particle size of the starting lepidocrocite and by increasing the residual pressure of water vapor. An interpretation of this behavior is given.

Introduction

The synthesis of nanosized γ-Fe_2O_3 has merited the attention of a large number of authors.[1−7] This is because of its great technological importance as a ferrofluid[8−10] and for its use in magnetic recording systems and magnetic pigments.[11−13] It is also worthy to note the recent increase in interest in growing nanosized γ-Fe_2O_3 inside a silica matrix in the development of magnetooptic devices for optical recording media.[12,14,15]

It is well-known[16] that ideal maghemite is a cation-deficient spinel with $21^1/_3$ Fe(III) ions distributed among 8 tetrahedral and 16 octahedral sites, where the $2^2/_3$ vacancies remaining in octahedral positions are randomly distributed. Thus, the unit cell formula is $(Fe_8^{3+})[Fe_{13^1/_3}^{3+}\ \square_{2^2/_3}]\ O_{32}$, where ( ) represents tetrahedral sites, [ ] octahedral sites, and □ stands for vacancies. This formula would be also written in the form $Fe_{2.67}\square_{0.33}O_4$, which points out that the structure of maghemite can be considered as that of magnetite with 12.5% of the Fe sites vacant.

The synthetic maghemites very often display superstructures forms[12,17] as a consequence of the ordering of the vacancies within the octahedral framework that depend on both its crystallite size and the amount of Fe^{2+} or other impurities in the structure.[12,18,19] The ordering of the vacancies is promoted by the presence of impurities and is inhibited as the crystal size decreases. The particle shape can also influence this

[†] Centro Mixto Universidad de Sevilla-C.S.I.C.
[‡] Institute of Inorganic Chemistry.

(1) Grimm, S.; Schultz, M.; Barth, S.; Müller, R. *J. Mater. Sci.* **1997**, *32*, 1083.
(2) Rouanet, A.; Solmon, H.; Pichelin, G.; Roucau, C.; Sibiende, F.; Monty, C. *Nanostruct. Mater.* **1995**, *6*, 283.
(3) Cabañas, M. V.; Vallet-Regi, M.; Labeau, M.; Gonzalez-Calbet, J. M. *J. Mater. Res.* **1993**, *8*, 2694.
(4) Verdaguer, S. V.; Morales, M. P.; Serna C. J. *Mater. Lett.* **1998**, *35*, 227.
(5) Martinez, B. M.; Roig, A.; Obradors, X.; Molins, E.; Rouanet, A.; Monty, C. *J. Appl. Phys.* **1996**, *79*, 2580.
(6) Vollath, D.; Szabó, D.; Taylor, R. D.; Willois, J. O. *J. Mater. Res.* **1997**, *12*, 2175.
(7) Kang, Y. S.; Risbud, S.; Rabolt, J. F.; Stroeve, P. *Chem. Mater.* **1996**, *8*, 2209.
(8) Raj, K.; Moskovitz, R. *J. Magn. Magn. Mater.* **1990**, *85*, 223.
(9) Sestier, C.; Dasilva, M. F.; Sabolovic, D.; Roger, J.; Pons, J. N. *Electrophoresis* **1998**, *19*, 1220.
(10) Gazoeau, F.; Bacri, J. C.; Gendron, F.; Perzynsky, R.; Raikher, Y. L.; Stepanov, V. I.; Dubois, E. *J. Magn. Magn. Mater.* **1998**, *186*, 157.
(11) Dorman, J. L.; Fiorani, D. *Magnetic properties of fine particles*; North-Holland; Amsterdam, 1992.
(12) Cornell, R. M.; Schwertmann, U. *The iron oxides*; VCH: Weinheim, 1996.
(13) Sharrok, M. P.; Bodnar, R. E. *J. Appl. Phys.* **1985**, *57*, 3919.
(14) Niznansky, D.; Rohspringer, J. L.; Drillon, M. *IEEE Trans. Magn.* **1994**, *30*, 821.
(15) Bentivegna, F.; Ferre, J.; Nyvlt, M.; Jannet, J. P.; Imhoff, D.; Canva, M.; Brun, A.; Veillet, P.; Visnovsky, S.; Chapat, F.; Boilot, J. P. *J. Appl. Phys.* **1998**, *83*, 7776.
(16) Waychunas, G. A. *Rev. Mineral.* **1991**, *25*, 11.
(17) Morales, M. P.; Pecharroman, C.; González-Carreño, T.; Serna, C. J. *J. Solid State Chem.* **1994**, *108*, 158.
(18) Bernal, J. D.; Dasgupta, D. R.; Mackay, A. L. *Clay Miner. Bull.* **1959**, *4*, 15.
(19) Feitknecht, W. *Rev. Pure Appl. Chem.* **1964**, 423.

10.1021/cm981062f CCC: $18.00
Published on Web 03/27/1999

ordering according to Morales et al.[17] These authors have reported that an increase in cation ordering is observed for γ-Fe_2O_3 as the axial ratio decreases, and the vacancies are completely ordered for spheres. Two kinds of vacancy ordering are assumed:[12,17] (1) an ordered distribution leading to a tetragonal symmetry [c/a = 3] and (2) as that of the lithium cation in the compound (Fe_8^{3+}) $[Li_4^+ Fe_{12}^{3+}]O_{32}$ with cubic symmetry. It has been proposed in the literature[12,20] that the latter structure is connected with the incorporation of water in the γ-Fe_2O_3 lattice, such that the proton occupy the vacant octahedral sites according to the formula (Fe_8^{3+})-$[H_4^+ Fe_{12}^{3+}]O_{32}$ that account for ~2% of water content.[21] Thus, it is generally assumed that the presence of water might have a stabilizing effect on maghemite because it contributes to an important decrease of the high level of vacancies in the structure.[20] However, Bakker et al. have concluded[22] that the thermal stability of maghemite obtained from the thermal decomposition of lepidocrocite, increases by decreasing its water content that, according to these authors, is correlated with the excess of H_2O molecules previously found for the corresponding precursor.

Maghemite is synthesized from solid-state transformations of another iron compound and generally adopts the habit of its precursor.[12] Thus, the conversions of the parent compounds into γ-Fe_2O_3 are generally considered topotactic transformations; the conversion of $N_2H_5Fe(N_2H_3COO)_3$ to γ-Fe_2O_3 reported by Morales et al.[23] constitutes a rare example where the maghemite crystals do not maintain the morphology of the precursor. Hence, the syntheses of precursors with very small particle sizes would be required for obtaining nanometric iron oxides samples. However, it must be pointed out that the crystallite size is not the only important factor influencing the properties of maghemite, but the particle shape is also a demanding factor for magnetic applications since it determines the shape anisotropy and then the coercive field value.[24] Thus, acicular-shaped particles of this material are required for longitudinal magnetic recording applications.[24,25] Maghemite cannot be directly obtained with such a shape, but lepidocrocite adopts this habit and can be transformed into γ-Fe_2O_3. Therefore, lepidocrocite is an excellent candidate for being used as starting material for the synthesis of acicular maghemite.

The thermal dehydration of lepidocrocite has merited the attention of many authors.[22,26−43] Wolska and Baszynsky,[41] Ghering et al.,[42,43] and Bakker et al.[22] have concluded from spectroscopic and magnetic studies that a molecular level prereactional dehydroxylation of the lepidocrocite begins at a temperature between 150 and 170 °C with the formation of superparamagnetic γ-Fe_2O_3 nuclei, although the overall conversion of γ-FeOOH to γ-Fe_2O_3 starts at about 200 °C. According to Naono et al.[40] the acicular crystals of lepidocrocite undergo a topotactic dehydroxylation, where the original single crystal of lepidocrocite is replaced by a highly ordered aggregate of small maghemite crystals with a large amount of micropores. The morphology of the original crystals is still maintained with the [001] axis and (100) plane of lepidocrocite corresponding to the [110] axis and the (001) plane of maghemite. The final product of the decomposition can be either γ-Fe_2O_3 or a mixture of maghemite and hematite, depending on the experimental conditions used for carrying out the thermal dehydroxylation of the lepidocrocite. Giovanolli and Brütsch[36] have concluded that the presence of water vapor induces nucleation of hematite, whereas under vacuum pure maghemite is obtained. It seems to be clear that the phase distribution in the final product obtained from the thermal decomposition of the lepidocrocite would depend on the thermal stability of the maghemite resulting from the topotactic dehydroxylation of the precursor.

It is generally assumed that maghemite is thermodynamically metastable with respect to hematite. The temperatures reported in the literature for the maghemite → hematite transformation range from 250 to 900 °C, depending on the synthesis method, crystallinity, impurity content, morphology of the particles, etc.[45,46] The published results concerning the influence of the particle size on the thermal stability of maghemite are contradictory. Thus, some authors[47,48] have concluded that the thermal stability of γ-Fe_2O_3 toward its transition to α-Fe_2O_3 decreases with increasing the particle size while, in contrast, other authors[22,49−51] consider that the stability of maghemite with regard to the polymorphic transformation increases with increasing the par-

(20) David, I.; Welch, A. J. E. *Trans. Farady Soc.* **1956**, *52*, 1642.
(21) Swaddle, T. W.; Oltmann, P. *Can. J. Chem.* **1980**, *58*, 1763.
(22) De Bakker, P. M. A.; De Grave, E. D.; Vandenberghe, R. E.; Bowen, L. H.; Pollard, R. J.; Persoons, R. M. *Phys. Chem. Miner.* **1991**, *18*, 331.
(23) Morales, J.; Tirado, J. L.; Valera, C. *J. Am. Ceram. Soc.* **1989**, *72*, 1244.
(24) Herrero, E.; Cabañas, M. V.; Vallet-Regi. M.; Martinez, J. L.; Gonzalez-Calbet, J. M. *Solid State Ionics* **1997**, *101*, 213.
(25) Ozaki, M.; Matijevic, E. *J. Colloid Interface Sci.* **1985**, *107*, 199.
(26) Hahn, F. L.; Hertrich, M. *Ver. Dtsch. Chem. Ges.* **1923**, *56*, 1729.
(27) Baudisch, O.; Albrecht, W. H. *J. Am. Ceram. Soc.* **1932**, *54*, 943.
(28) Goldztaub. S. *Bull. Soc. Fr. Miner. Cristallogr.* **1935**, *58*, 6.
(29) Glemser, O. *Ver. Dtsch. Chem. Ges.* **1938**, *71*, 158.
(30) Bernal J. D.; Desgupta, D. R.; Mackay, A. L. *Nature* **1957**, *180*, 645.
(31) Takada, T.; Kiyama, M.; Shimizu, S. *Bull. Inst. Chem. Res. Kyoto Univ.* **1964**, *42*, 505.
(32) Takada, T.; Nagasawa, K.; Kiyama, M.; Shimizu, S.; Bando, Y. *Bull. Inst. Chem. Res. Kyoto Univ.* **1969**, *47*, 600.
(33) Ishikawa, T.; Inouye, K. *Bull. Chem. Soc. Jpn.* **1972**, *45*, 2530.
(34) Ishikawa, T.; Inouye, K. *Bull. Chem. Soc. Jpn.* **1973**, *46*, 2665.
(35) Giovanolli, R.; Brütsch, R. *Chimia* **1974**, *28*, 188.
(36) Giovanolli, R.; Brütsch, R. *Thermochim. Acta* **1975**, *13*, 15.
(37) Subrt, J.; Hanousek, F.; Zapletal, V.; Lipka, J.; Hucl, M. *J. Therm. Anal.* **1981**, *20*, 61.
(38) Gomez-Villacieros, R.; Hernán, L.; Morales, J.; Tirado, J. L. *J. Colloid Interface Sci.* **1984**, *101*, 392.
(39) Morris, R. V.; Lauer, H. V.; Lawson, C. A.; Gibson, E. K.; Nace, G. A.; Stewart, C. *J. Geophys. Res.* **1985**, *90*, 3126.
(40) Naono, H.; Nakai, K. *J. Colloid Interface Sci.* **1989**, *128*, 146.
(41) Wolska, E.; Bazynsky, J. *Phys. Status Solidi (A)* **1986**, *95*, 87.
(42) Ghering, A. U.; Karthein, R.; Reller, A. *Naturwissenschaften* **1990**, *77*, 177.
(43) Gehring, A. U.; Hofmeister, A. M. *Clays Clay Miner.* **1994**, *42*, 409.
(44) Koga, N.; Okada, S.; Nakamura, T.; Tanaka, H. **1995**, *267*, 195.
(45) De Böer, C. B.; Dekkers, M. J. *Geophys. Res. Lett.* **1996**, *23*, 2815.
(46) Bate, G. Recording Materials. In *Ferromagnetic materials*; Wohlfart, E. P., Ed.; North-Holland: New York, 1980; pp 381−507.
(47) Vajpei, A. C.; Mathieu, F.; Rousset, A.; Chassagneus, F.; Letoffe, J. M.; Claudy, P. *J. Therm. Anal.* **1987**, *32*, 857.
(48) Grimm, S.; Stelzner, T.; Leuthäusser, J.; Barth, S.; Heide, K. *Thermochim. Acta* **1997**, *300*, 141.
(49) Feitknecht, W.; Michelis, W. *Helv. Chim. Acta* **1962**, *45*, 212.
(50) De Biasi, R. S.; Portella, P. D. *Phys. Rev. B* **1980**, *22*, 304.
(51) Chhabra, V.; Lal, M.; Maitra, A. N.; Ayyub, P. *Colloid Polym. Sci.* **1995**, *273*, 939.

ticle size. However, it is worthy to note that the sets of maghemite samples with different particle size used in previous papers for studying the influence of this parameter on its thermal stability have been synthesized in every case from different precursors. Therefore, these results can be influenced not only by the particle size but also by the different shapes and impurities of the maghemite particles obtained from the different precursors.

The scope of the present work is to study the influence of the particle size of a set of acicular lepidocrocite samples on the texture, structure, and thermal stability of the iron oxide obtained as final product. The lepidocrocite samples used here have been synthesized in a similar way to achieve the same purity for all the starting samples. The method of Constant Rate Thermal Analysis (CRTA) has been used for monitoring the thermal decomposition of the lepidocrocite. This technique uses a feedback from the sample reaction itself to input into the algorithm governing the furnace control. Thus, the reaction temperature is monitored in such a way that both the reaction rate and the partial pressure of water vapor generated during the thermal dehydroxylation of the lepidocrocite are maintained constant at the value previously selected by the user. This method would allow the influence of both the particle size of the precursor and the partial pressure of water vapor on the texture and structure of the iron oxide obtained to be discerned. The CRTA method has been previously used for controlling the texture and structure of some materials through the kinetic control of the thermal decomposition of their corresponding precursors.[52−56] The results reported here constitute the first attempt of using the CRTA method for controlling the texture and structure of the final products obtained from the thermal decomposition of the lepidocrocite.

Experimental Section

Materials. Two lepidocrocite samples have been used, L-92 and L-43 with a specific surface of 92 and 43 $m^2\ g^{-1}$, respectively.

The sample L-92 was prepared by air oxidation of an $FeSO_4$ solution obtained by dissolution of 300 g of $FeSO_4 \cdot 7H_2O$ in 4 L of distilled water acidified by 2 drops of 96% H_2SO_4. The oxidation reaction was carried out at a constant pH value of 7.5 in the temperature range 20−25 °C. The pH value was maintained at a constant during oxidation by continuous addition of 13.5% aqueous NH_3. The airflow rate was controlled in such a way that the total oxidation was achieved in 1 h. The obtained lepidocrocite precipitate was filtered off, washed with distilled water, and dried at room temperature.

The first step of preparation of the L-43 sample was identical to the L-93 one, but the γ-FeOOH suspension obtained was used as nuclei for growing larger lepidocrocite crystals. Thus, 400 g of $FeSO_4 \cdot 7H_2O$ was added to this γ-FeOOH suspension after adjusting the pH value to 4.5 and the temperature to 45 °C. The airflow rate was selected such that the total oxidation of Fe^{2+} to Fe^{3+} takes place in 3 h. The addition and oxidation of 400 g of $FeSO_4 \cdot 7H_2O$ was then repeated at the same conditions. The obtained lepidocrocite precipitate was filtered off, washed with distilled water, and dried at room temperature.

Table 1. Phase Composition Calculated from the Mössbauer Spectra[a]

atmosphere	α-Fe_2O_3 (%)	γ-Fe_2O_3 (%)
dry helium	9	91
humid helium	49	51

[a] Spectra were obtained for the samples resulting from the thermal decomposition of the L-43 lepidocrocite sample under a flow of dry and humid helium, respectively.

Methods. The powder X-ray diffraction spectra (XRD) of the samples were obtained with a Philips PW 1060 instrument equipped with a scintillation counter, Cu Kα radiation and a nickel filter. The size of the coherently diffracting domains of samples was determined from the analysis by Scherrer's method.

^{57}Fe Mössbauer spectra were recorded at room temperature in transmission geometry by using a source of ^{59}Co in a Cr matrix moving in constant acceleration regime. Isomer shifts were referred to α-Fe. The spectra were fitted by computing up to six sextets, in addition to a doublet and a singlet generally attributable to the phases possibly present in the sample. During the fitting procedure the following quantities were left free: the line widths and their distributions, quadrupole splitting, isomer shift, and hyperfine field.

The Mössbauer spectra of all samples showed presence only of magnetically ordered components. The nonsymmetrical lines broadened toward the center of the spectrum could not be satisfactorily fitted with only one sextet. This indicates that the phases present in the products consist of very small particles, indicating signs of superparamagnetic behavior. The main component found in spectra of all measured samples corresponds to γ-Fe_2O_3 (maghemite) consisting of very small particles with broad particle size distribution.[22,37] To fit this component satisfactorily, 4−6 sextets with B_{Hf} values in the range 18.8−47.6 T were necessary.[22] The content of γ-Fe_2O_3 (maghemite) given in the Table 1 corresponds to the sum of area of these sextets. The second significant magnetically ordered component found in some samples was satisfactorily covered with only one sextet with B_{Hf} value in the range 45.3−51.3 T, QS in range −0.11/−0.22, and IS in range 0.34−0.41. These values correspond rather well to the literature data for small defect particles of α-Fe_2O_3 (hematite).[57−59]

The specific surface area was measured by the BET method using a Micromeritics surface area, model 2200.

Transmission electron microscopy (TEM) was carried out in a Philips CM 200 microscope working at 200 kV.

The DSC experiments were carried out in a Setaram DSC 111 equipment with a maximum sensitivity of 1 μJ s^{-1}. A helium flow of 40 $cm^3\ min^{-1}$ and a heating rate of 10 K min^{-1} were used.

To study the texture and structure of the products obtained from the thermal decomposition of lepidocrocite, some experiments were carried out using a linear heating program under vacuum or controlled atmosphere. In addition, the thermal decomposition of lepidocrocite was carried out under vacuum by means of the Constant Rate Thermal Analysis method (CRTA). This method implies to control the reaction temperature in such a way that both the pressure of the gases generated in the reaction and the total decomposition rate remain constant at values previously selected by the user. The experimental tool developed in this work has been described elsewhere.[53,54] It basically consists of a conventional vacuum

(52) Rouquerol, J.; Rouquerol, F.; Gantaume, M. *J. Catal.* **1979**, *57*, 522.
(53) Criado, J. M.; Gotor, F. J.; Real, C.; Jimenez, F.; Ramos, S.; Del Cerro J. *Ferroelectrics* **1991**, *115*, 43.
(54) Gotor, F. J.; Real, C.; Dianez, M. J.; Criado, J. M. *J. Solid State Chem.* **1996**, *123*, 331.
(55) Bordère, S.; Lewellyn, P. L.; Rouquerol F.; Rouquerol, J. *Langmuir* **1998**, *14*, 4217.
(56) Gotor, F. J.; Macías, M.; Ortega, A.; Criado, J. M. *Int. J. Chem. Kinet.* **1998**, *30*, 647.
(57) Murad, E.; Johnston, J. H. Iron Oxides and Oxhydroxides. In *Mössbauer Spectroscopy Applied to Inorganic Chemistry;* Long, G. J., Ed.; Plenum Publ. Corp; New York, 1987; Vol. 2, pp 507−581.
(58) Chadwick, J.; Jones, D. H.; Thomas, M. F.; Tatlock, G. J.; Devenish, R. W. *J. Magn. Magn. Mater.* **1986**, *59*, 301.
(59) Tsui, T.; Naito, K.; Ishigure, K. *Phys. Status Solidi (A)* **1984**, *82*, K57.

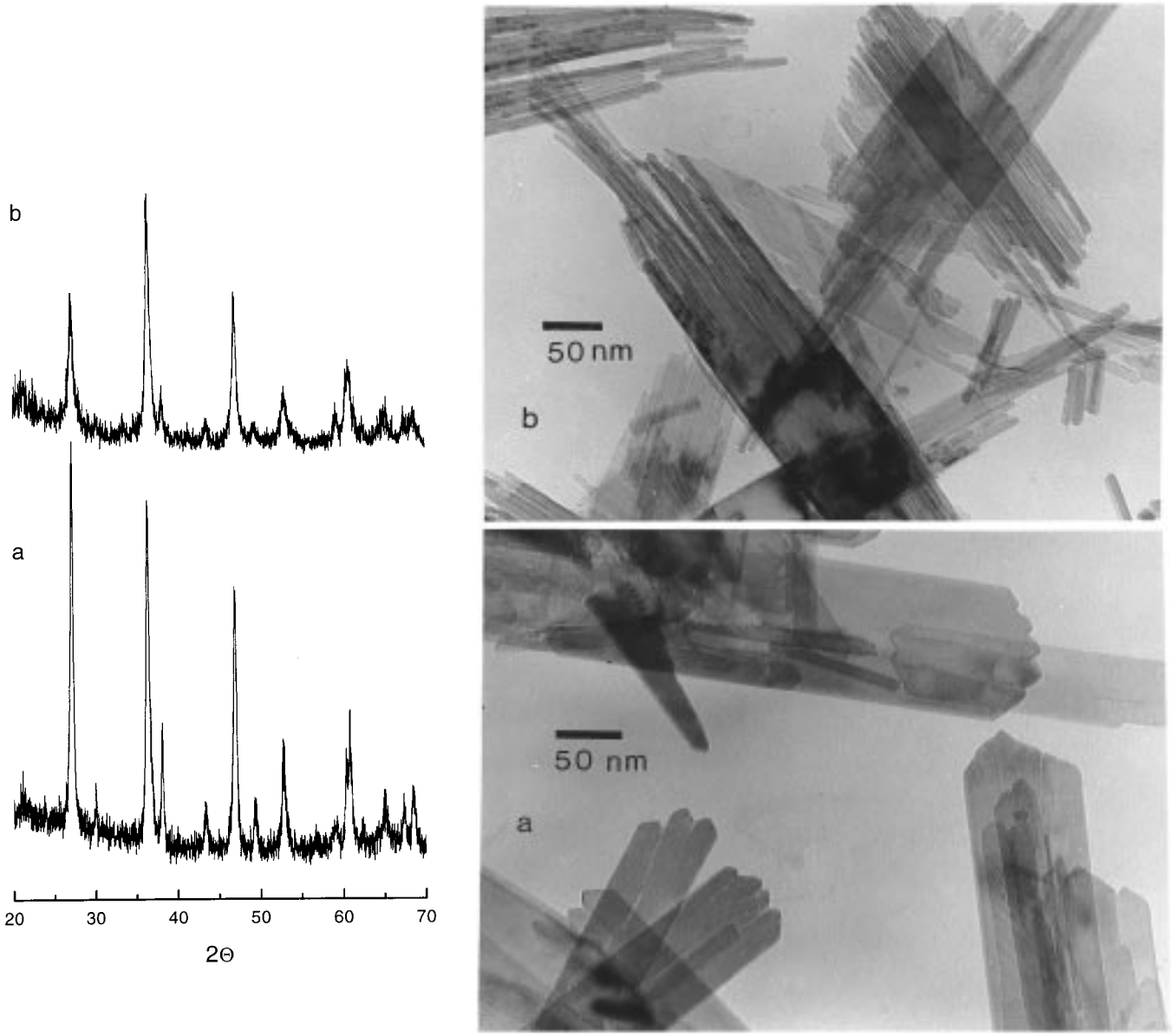

Figure 1. XRD diagrams and TEM pictures of the starting lepidocrocite samples: (a) L-43 and (b) L-92.

apparatus equipped with a Penning and a Pirani gauges that are interfaced to the sample heater through a PID temperature controller. The pressure (P) is kept constant at a value previously selected by the user in the range from 10^{-5} to 10 mbar. Moreover, the pumping rate of the vacuum system can be controlled by means of a vacuum valve at the time that the pressure is maintained constant at the previously selected value. Thus, provided that both the pressure and the pumping rate are kept constants, the rate at which the gases generated in the decomposition reaction are evolved must be maintained constant all over the process. The constant decomposition rate, C, represents the fraction of solid reacted per minute and, therefore, C^{-1} accounts for the time at which decomposition of lepidocrocite is completed.

Results and Discussion

Figure 1 shows the XRD diagrams of L-43 and L-92 lepidocrocite samples, respectively. γ-FeOOH has been the only crystalline phase identified in both samples. TEM pictures also shown in Figure 1 suggest that L-43 sample is constituted by lath-like particles while the L-92 sample consists of bundles of thin needle-shaped crystals. It can be observed that the average width of the crystals of the L-43 sample is considerably larger than that of the L-92 sample. These results are consistent with those obtained from BET specific surface measurements (L-43 42.5 $m^2\ g^{-1}$; L-92 91.5 $m^2\ g^{-1}$).

Parts a and b of Figure 2 show the XRD diagrams of the Fe_2O_3 obtained from the thermal decomposition of L-43 lepidocrocite sample at a linear heating rate of 0.2 °C min^{-1} under open atmosphere and a helium flow of 100 $cm^3\ min^{-1}$, respectively. The temperature was raised to 350 °C and maintained at this value for 2 h in both experiments. It can be observed that the final product obtained from the thermal decomposition of lepidocrocite under helium is mainly constituted by γ-Fe_2O_3 while the product obtained under open air contains an appreciable amount of α-Fe_2O_3. We must bear in mind that the isostructural character of γ-Fe_2O_3 and Fe_3O_4 makes difficult to distinguish these phases from X-ray diffraction. Thus, the results obtained under flowing helium could be also interpreted by considering

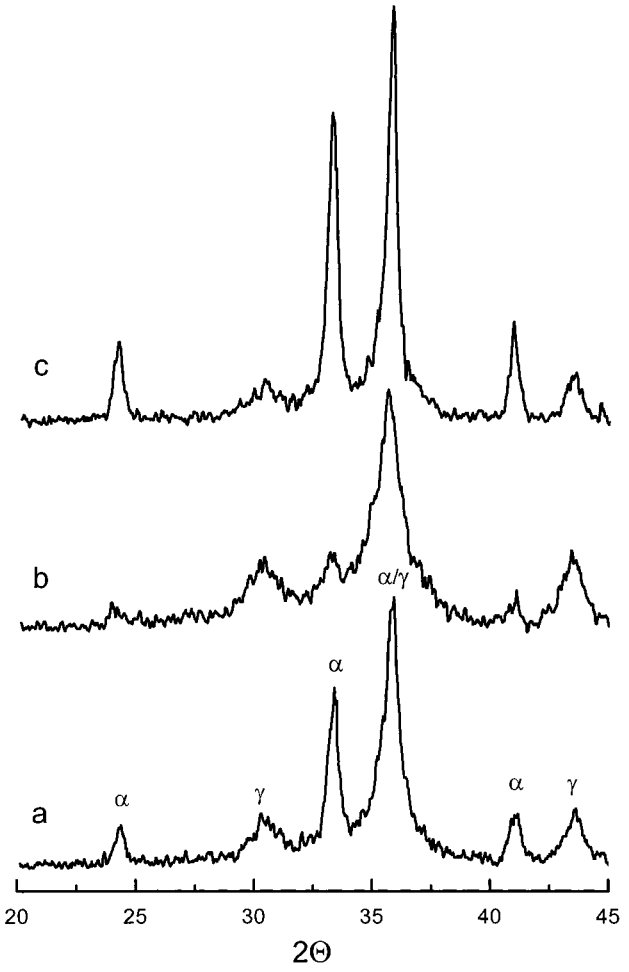

Figure 2. XRD diagrams of the final products obtained from the thermal decomposition of the L-43 lepidocrocite recorded under different atmospheres at a heating rate of 0.2 K min^{-1}: (a) open air atmosphere, (b) dry helium flow, and (c) flow of helium saturated with water vapor at room temperature.

the formation of magnetite, provided that according to Wells,[60] Fe_2O_3 could be converted into Fe_3O_4 by heating from 250 °C in absence of oxygen (i.e., under vacuum). In summary, the above results could be explained considering that oxygen and/or water vapor favor the stabilization of α-Fe_2O_3. We must bear in mind that helium flow purges oxygen and also removes the water vapor generated in the reaction from the close vicinity of the sample. It would be interesting to discern if the formation of α-Fe_2O_3 is promoted either by the oxygen or by the water vapor. Thus, it has been analyzed an additional iron oxide sample obtained by decomposing the L-43 lepidocrocite at the same heating rate of 0.2 °C min^{-1} but using a flow of helium saturated with water vapor instead of dry helium. The XRD diagram of the sample, included in Figure 2c, suggests that the pressure of water vapor enhances the formation of hematite, according to Giovanolli and Brütsch.[36] Hence, it is reasonable to assume that maghemite instead of magnetite is obtained from the thermal decomposition of lepidocrocite in the presence of water vapor.

Figure 3 shows the Mössbauer spectra recorded for the two iron oxide samples obtained for the thermal

(60) Wells, A. F. *Structural Inorganic Chemistry*, 5th ed.; Oxford University Press: Oxford, 1984; p 491.

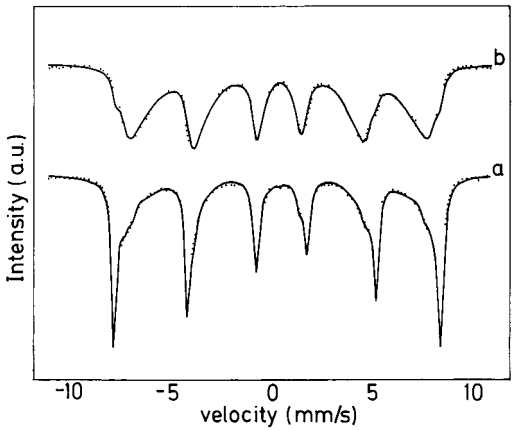

Figure 3. Mössbauer spectra of lepidocrocite thermal decomposition products prepared under dry (a) and humid helium (b), respectively.

decomposition of lepidocrocite under dry and humid helium, respectively, as previously described. The analysis of the Mössbauer spectra indicates that magnetite has not been formed and exclusively γ-Fe_2O_3 (maghemite) and α-Fe_2O_3 (hematite) constitute the samples. The percentages calculated for both phases are included in Table 1. These data point out that the percentage of α-Fe_2O_3 obtained from the thermal decomposition of lepidocrocite ranges from 9%, if the reaction is conducted under dry helium, to 49%, if the thermal decomposition of the precursor occurs under water vapor atmosphere.

Taking into account the above considerations it would be interesting to carry out a careful analysis of the influence of the decomposition rate and the partial pressure of water vapor on both the morphology and the composition, i.e., α-Fe_2O_3/γ-Fe_2O_3 ratio, obtained from the thermal decomposition of lepidocrocite. The CRTA method has been used for this purpose. This method allows the temperature of the sample to be controlled in such a way that both the partial pressure of the water vapor self-generated in the thermal decomposition of lepidocrocite and the decomposition rate of this compound are maintained constant at values previously selected by the user. The values of the reacted fraction, α, calculated from the CRTA curves have been plotted as a function of T in Figure 4. Figure 4a shows the α-T plots obtained for the decomposition of the L-43 lepidocrocite sample by means of the CRTA method at a constant water vapor partial pressure $p = 5 \times 10^{-5}$ mbar and different decomposition rates. It is shown that the lower the decomposition rate selected, the lower the temperature at which the decomposition takes place. This behavior can be easily understood if we take into account[56] that the rate of a solid-state reaction can be described by the general equation:

$$\frac{d\alpha}{dt} = Ae^{-E/RT} f(\alpha) \qquad (1)$$

where α is the reacted fraction at the time t; A is the preexponential factor of Arrhenius; E is the activation energy; T is the absolute temperature; and $f(\alpha)$ is a monotonic function depending on the kinetic law obeyed by the reaction whose absolute value increases by increasing α. If the process is carried out at a constant

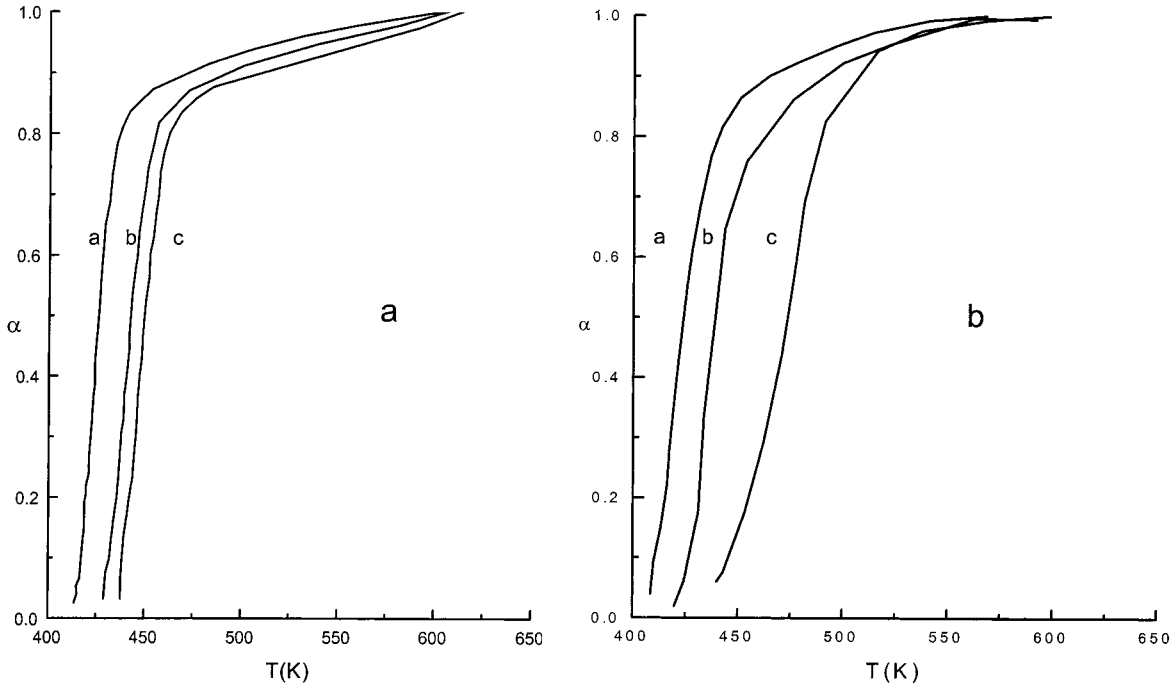

Figure 4. CRTA plots obtained for the thermal decomposition of the L-43 lepidocrocite sample: (A) under a constant water vapor pressure of 5×10^{-5} mbar and various constant decomposition rates [(a) 4×10^{-4} min^{-1}; (b) 1.8×10^{-3} min^{-1}; (c) 3.9×10^{-3} min^{-1}] and (B) at a constant decomposition rate $C \cong 1.6 \times 10^{-3}$ min^{-1} and various constant residual pressures of water vapor [(a) 5×10^{-5} mbar; (b) 5×10^{-1} mbar (c) 8.2 mbar].

reaction rate $C = \mathrm{d}\alpha/\mathrm{d}t$, eq 1 can be written in the form:

$$C = A\mathrm{e}^{-E/RT} f(\alpha) \qquad (2)$$

Thus, the higher C is the higher must be the temperature at which a particular value of α is reached, provided that eq 2 must be fulfilled.

The influence of the partial pressure of water vapor on the thermal decomposition of γ-FeOOH is shown in Figure 4b. This figure represents a set of α-T plots recorded at a constant decomposition rate $C = 1.6 \times 10^{-3}$ min^{-1} but at different selected values for the pressure of the water vapor produced in the reaction. It can be observed that the decomposition temperature of lepidocrocite decreases by decreasing the partial pressure of water vapor. It is noteworthy that under a constant pressure of 5×10^{-5} mbar the reaction is over at 195 °C that, to our knowledge, is considerably lower than any other previously reported in the literature. Thus, Koga et al.[44] have reported that the dehydroxylation of needle-shaped γ-FeOOH samples, similar in size and shape to those described in Figure 1, starts at temperatures higher than 220 °C. Moreover, Goehring et al.[43] have concluded in recent papers that the thermal decomposition of lepidocrocite takes place through a mechanism that implies the previous formation of superparamagnetic γ-Fe_2O_3 clusters, which starts close to 175 °C and is completed around 300 °C. The results obtained in the present paper suggest that the range of temperatures previously reported in the literature for the thermal decomposition of lepidocrocite seems to be more representative of the experimental conditions used than of the morphological features of the samples.

A set of iron oxide samples have been obtained from the thermal decomposition of the L-43 lepidocrocite by means of the CRTA method at different water vapor pressures and constant decomposition rates, C. Once the decomposition was over, the sample temperature was allowed to increase to 350 °C under high vacuum and held at this temperature for 2 h before cooling to room temperature and exposing to the air atmosphere. The reason for this standard thermal treatment for the whole series of samples was to make sure that their phase compositions depend only on the experimental conditions used for the thermal decomposition of lepidocrocite rather than on the final temperature reached by the sample. The XRD diagrams of the final products obtained from the thermal decomposition of the L-43 lepidocrocite sample are shown in Figure 5. It can be observed that the amount of hematite increases by increasing the partial pressure of water vapor and it is independent of the decomposition rate. Moreover, the TEM pictures for the γ-Fe_2O_3, yielded from the thermal decomposition of the L-43 lepidocrocite sample under a vacuum of 5×10^{-5} mbar and 8.2 mbar, are also shown in Figure 5. The specific surfaces of the samples obtained have been measured and the ratios between their actual values, S, and the specific area, S_0, of the γ-FeOOH precursor have been plotted in Figure 6 as a function of the decomposition rate. It can be observed that the S/S_0 ratio dramatically increases by decreasing the constant pressure selected for carrying out the thermal decomposition of lepidocrocite. However, the influence of the decomposition rate, C, is not important when compared with the influence of the partial pressure of water vapor. It has been concluded in the literature[40] that the shape and size of needle-shaped lepidocrocite is preserved after its thermal decomposition leading to a microporous needle-shaped γ-Fe_2O_3. The TEM pictures in Figure 5 confirm the above conclusion. The size and shape of the precursor seem to be maintained. Moreover, a large number of round pores randomly distributed across the plate-like particle

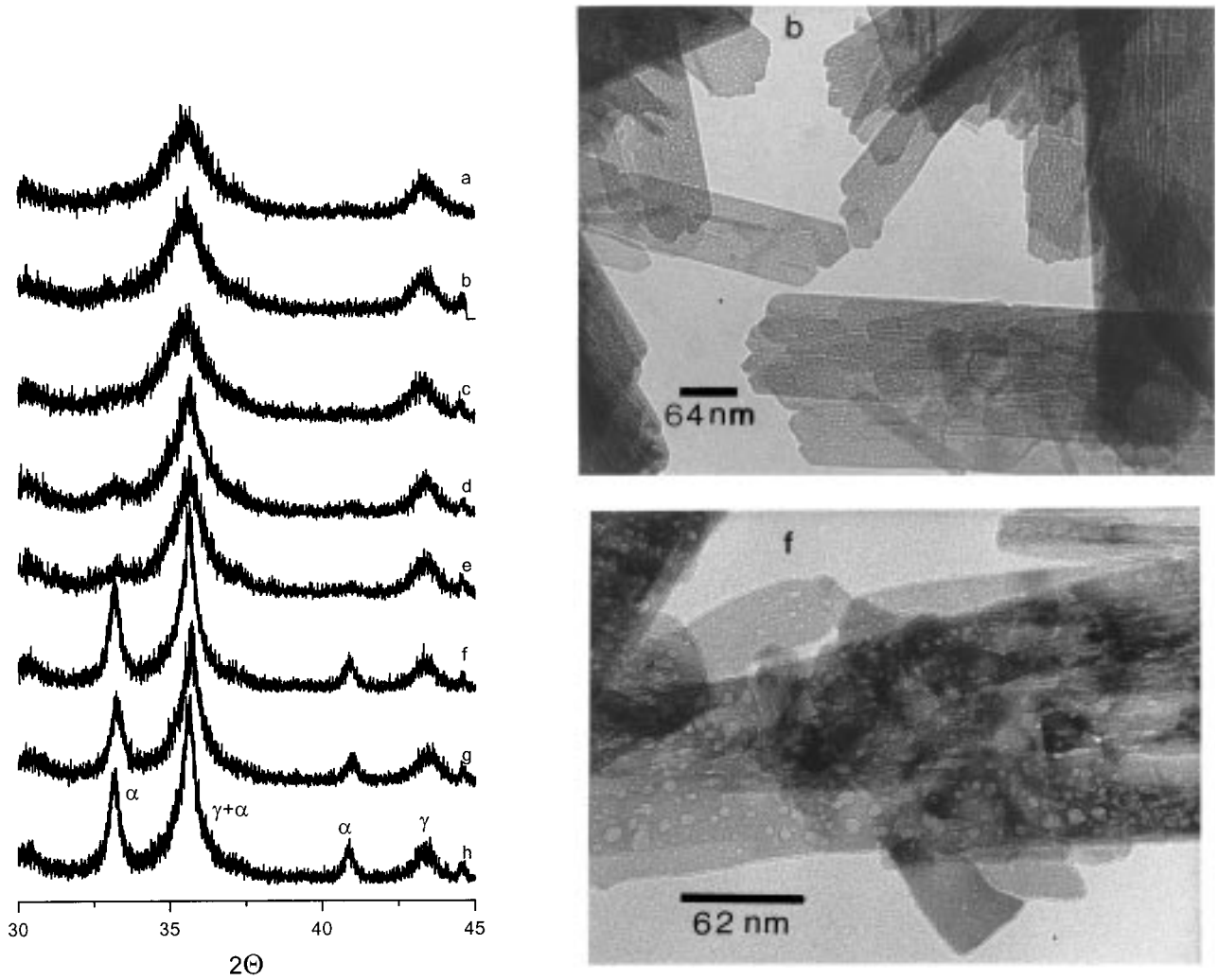

Figure 5. XRD diagrams and TEM pictures of the final products obtained from the thermal decomposition of L-43 lepidocrocite (1) at a constant residual pressure of water vapor equal to 5×10^{-5} mbar and different values of C [(a) 2×10^{-4} min^{-1}; (b) 1.8×10^{-3} min^{-1}; (c) 3.9×10^{-3} min^{-1}]; (2) at a constant residual pressure equal to 5×10^{-1} mbar and different values of C [(d) 6×10^{-4} min^{-1}; (e) 1.2×10^{-3} min^{-1}]; and (3) at a constant partial pressure of water vapor equal to 8.2 mbar and the following values of C [(f) 1.7×10^{-3} min^{-1}; (g) 3.1×10^{-3} min^{-1}; (h) 5.6×10^{-3} min^{-1}].

have been generated, as compared with the picture of the original L-43 sample shown in Figure 1a. In other words, it seems to be clear that the "holes" (pores) shown in Figure 5 for the dehydrated lepidocrocite sample were not previously observed in the micrograph shown in Figure 1a for the starting nondehydrated lepidocrocite sample. Thus, it would be reasonable to conclude that these "holes" have been generated as a consequence of the dehydration of lepidocrocite. Taking into account the above considerations, the increase of the specific surface during the thermal decomposition of lepidocrocite would be ascribed to internal surface generated by the developed porosity. The results reported in Figure 6 would be interpreted by considering that the porosity generated during the thermal decomposition of lepidocrocite increases by decreasing the partial pressure of water vapor.

The analysis of the Mössbauer spectra of these samples included in Figure 7 are in good agreement with the corresponding X-ray results. The phase compositions calculated from these spectra for the iron oxides obtained from the thermal decomposition of the L-43 lepidocrocite sample under different experimental conditions, by means of the CRTA method, are shown in Table 2. It can be observed that the phase composition moves from almost pure maghemite, if the precursor is decomposed under a constant pressure of water vapor as low as 5×10^{-5} mbar, down to 63%, if the water vapor pressure is increased up to 8.2 mbar. Table 1 shows that the maghemite percentage in the final product is still decreased to 51% by decomposing the L-43 lepidocrocite precursor under a flow of helium saturated with water vapor at room temperature. A partial pressure of water vapor higher than 18 mbar would be expected under these experimental conditions. In summary, the results here reported clearly show that the percentage of maghemite obtained from the thermal decomposition of the L-43 lepidocrocite sample decreases by increasing the water vapor pressure in the close vicinity of the sample. Moreover, the analysis of the broadening of the (311) XRD peak of maghemite phase of these samples by the Scherrer's method indicates that the γ-Fe_2O_3 crystallite size decreases by decreasing the constant partial pressure of water vapor selected for decomposing the oxyhydroxide precursor. These results are consistent with the fact that the porosity dramatically increases

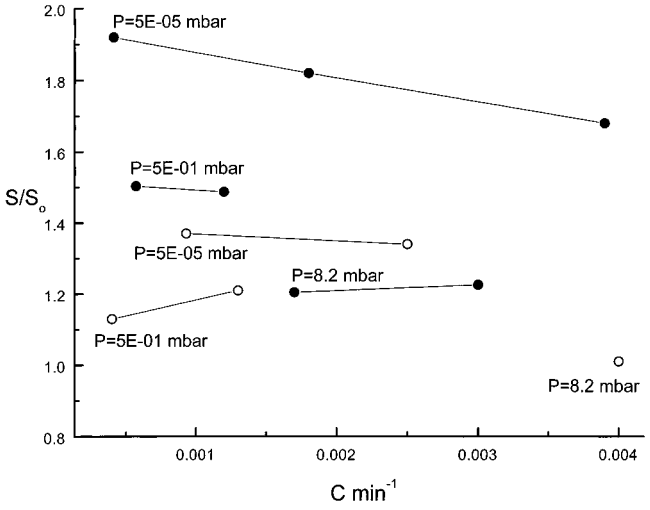

Figure 6. Ratio between the specific surface of iron oxides, S, and the surface area of the corresponding precursors, S_0, represented as a function of the decomposition rate, for different values of the residual pressure of water vapor maintained constant during the thermal decomposition of lepidocrocite. Precursors: (●) L-43; (○) L-92.

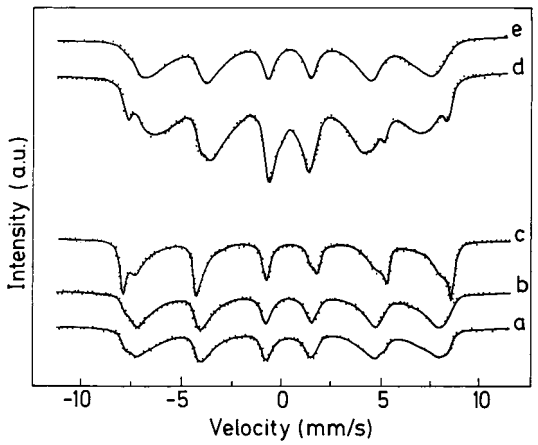

Figure 7. Mössbauer spectra recorded for the iron oxides obtained from the thermal decomposition of the L-43 and L-92 lepidocrocite precursors under different constant decomposition rates, C, and constant residual pressures of water vapor as selected by means of the CRTA method. Ex-L-43 samples: (a) P = 5×10^{-5} mbar and $C = 4 \times 10^{-4}$ min^{-1}; (b) P = 0.5 mbar and $C = 1.2 \times 10^{-3}$ min^{-1}; (c) $P = 8.2$ mbar and $c = 1.7 \times 10^{-3}$ min^{-1}. Ex-L-92 samples: (d) $P = 5 \times 10^{-5}$ mbar and C $= 9.3 \times 10^{-4}$ min^{-1}; (e) $P = 8.2$ mbar and $C = 4 \times 10^{-3}$ min^{-1}.

by decreasing the partial pressure of water vapor. This behavior suggests that the pores generated divide the particles in small crystals; in other words, it is reasonable to expect a decrease in the crystallite size by increasing the porosity according to our finding. On the other hand, it is worthy to note that the results obtained show that the higher the broadening of the maghemite XRD peaks is, the higher the percentage of γ-Fe_2O_3 formed. This fact suggests that the maghemite stability increases either by decreasing the crystallite size or by increasing the microstrains generated by the porous system.

A set of iron oxide samples obtained from the thermal decomposition of the L-92 sample by means of the CRTA method, in a similar way as previously described for the L-43 sample, have been studied. The XRD diagrams recorded for the iron oxide samples obtained from the thermal decomposition of the L-92 lepidocrocite are included in Figure 8. It can be observed that maghemite is the phase mainly detected regardless of conditions, i.e., decomposition rate and water vapor partial pressure, were selected. The TEM pictures of the iron oxide samples obtained by decomposing the L-92 lepidocrocite precursor by means of the CRTA method under a partial pressure of 5×10^{-5} mbar and 8.2 mbar, respectively, are also shown in Figure 8. The comparison of these pictures with those included in Figure 1 points out that porous particles that maintain both the size and the needle shape of the precursor are obtained.

The ratio between the specific surface of the iron oxide, S, and the specific area of the L-92 lepidocrocite precursor, S_0, have been calculated for the three series of samples obtained at different water vapor partial pressures. The values obtained have been plotted as a function of the decomposition rate in Figure 6. These results show that the S/S_0 ratio is independent of C but increases by decreasing the partial pressure of water vapor in a similar way as previously reported for the ex-L-43 γ-FeOOH samples, these results are in good agreement with the TEM pictures shown in Figure 8.

The Mössbauer spectra shown in Figure 7 confirm that these samples mainly consist of γ-Fe_2O_3. The hematite percentage in the sample has been estimated to be around 10% for all the samples, although an accurate determination has not been possible because the large broadening of the Mössbauer spectra bands. The crystal sizes, as determined from the broadening of the (311) maghemite peak, are included in Table 2. It can be observed that the particle size ranges from 7 to 4.0 nm and decreases by decreasing the partial pressure of water vapor selected for decomposing the L-92 lepidocrocite sample. However, Table 2 shows that the crystallite size of the γ-Fe_2O_3 obtained from the decomposition of this sample under a water vapor pressure of 8.2 mbar is considerably smaller than the crystal size obtained at this pressure from the thermal decomposition of the L-43 lepidocrocite precursor.

The results concerning the texture and microstructure of the iron oxide obtained from the thermal decomposition of lepidocrocite could be interpreted by considering that the lower the maghemite crystallite size is the higher its stability toward the transformation to hematite. In fact the iron oxide samples with crystallite sizes smaller than 6.5 nm consist of pure maghemite while the samples with higher maghemite crystallite sizes contain an important percentage of hematite. These results perhaps could be alternatively interpreted as a function of the difference in the strain energy stored by the maghemite obtained by using either the L-43 or the L-92 lepidocrocite samples as precursors.

To check if the thermal stability of γ-Fe_2O_3 phase depends only on its crystallite size it has been considered of interest to compare the temperature of the γ-$Fe_2O_3 \rightarrow \alpha$-$Fe_2O_3$ phase transition of a series of maghemite samples properly selected among those synthesized in this work. Figure 9 shows the DSC diagrams of the γ-Fe_2O_3 samples obtained from the thermal decomposition of the L-43 lepidocrocite sample under a water vapor pressure of 5×10^{-5} mbar and 8.2 mbar, respectively. It can be observed that the transition temperatures of both samples are practically identical

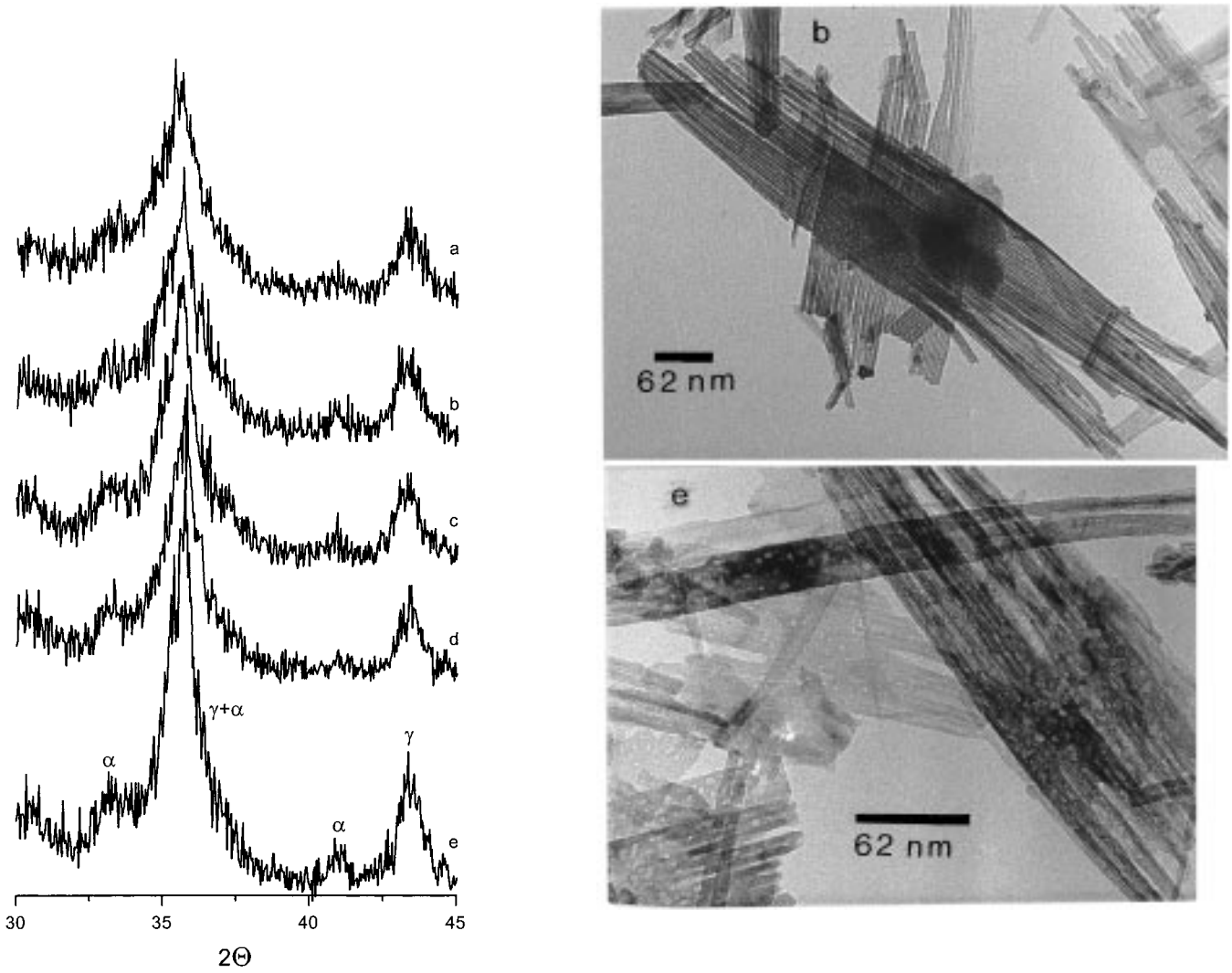

Figure 8. XRD diagrams and TEM pictures of the final products obtained from the thermal decomposition of L-92 lepidocrocite by CRTA at different values of the constant decomposition rate, C, and the constant residual pressure of water vapor. $P = 5 \times 10^{-5}$ mbar and the following values of C: (a) 9.3×10^{-4} min^{-1}; (b) 2.5×10^{-3} min^{-1}. $P = 5 \times 10^{-1}$ mbar and the following values of C: (c) 1.4×10^{-4} min^{-1}; (d) 1.3×10^{-3} min^{-1}. **(e)** $P = 8.2$ mbar and $C = 4 \times 10^{-3}$ min^{-1}.

Table 2. Specific Surface (S_{BET}), Phase Composition, Crystallite Size (D_{311}), and Transition Enthalpy (ΔH_t) of Maghemite Phase Determined for the Samples Obtained from the Thermal Decomposition of the Precursors L-43 and L-92 under Different Constant Values of Both Partial Pressure of Water Vapor (P) and Decomposition Rate (C)

precursor	C (min^{-1})	P (mbar)	D_{311} (nm)	S_{BET} (m^2 g^{-1})	% Mag.	% Hem	ΔH_t (KJ mol^{-1})
L-43	4.0×10^{-4}	5×10^{-5}	4	81.5	95	5	20
	1.2×10^{-3}	5×10^{-1}	5	63.9	95	5	–
	1.7×10^{-3}	8.2	10	52.1	63	37	21
L-92	9.3×10^{-4}	5×10^{-5}	4	125	≃90	≃10	12
	1.4×10^{-4}	5×10^{-1}	6	103.3	–	–	–
	4.1×10^{-3}	8.2	7	92.5	≃90	≃10	13

despite, as Table 2 shows, having different crystallite sizes. The γ-$Fe_2O_3 \rightarrow \alpha$-$Fe_2O_3$ transition (GAT) enthalpies have been calculated from the above diagrams after taking into account the real percentage of maghemite transformed into hematite previously contained in the sample. The results obtained are shown in Table 2. The values closed to 20 kJ mol^{-1} obtained for both samples roughly agree with the value of 25.3 kJ mol^{-1} recently reported by Diakonov[61] for the GAT enthalpy. However, it must be pointed out that according to the Diakonov's review, the values previously reported in the literature for this parameter scatter from 15 to 25.5 kJ mol^{-1}.

The DSC diagrams recorded for the maghemite obtained from the thermal decomposition of the L-92 precursor under water vapor partial pressures of 5×10^{-5} mbar and 8.2 mbar, respectively, are included in Figure 9. Table 2 shows the GAT enthalpy calculated from these diagrams, after assuming that the γ-Fe_2O_3 in the samples amounts for 90%, according to the results obtained from Mössbauer spectroscopy. These results point out that the phase transition temperature of these two ex-L-92 samples are very similar between themselves but considerably higher than those obtained for the maghemite samples obtained from the L-43 lepidocrocite precursor. Moreover, Table 2 shows that the enthalpy released during the phase conversion of the

(61) Diakonov, I. I. *Eur. J. Mineral.* **1998**, *10*, 17.

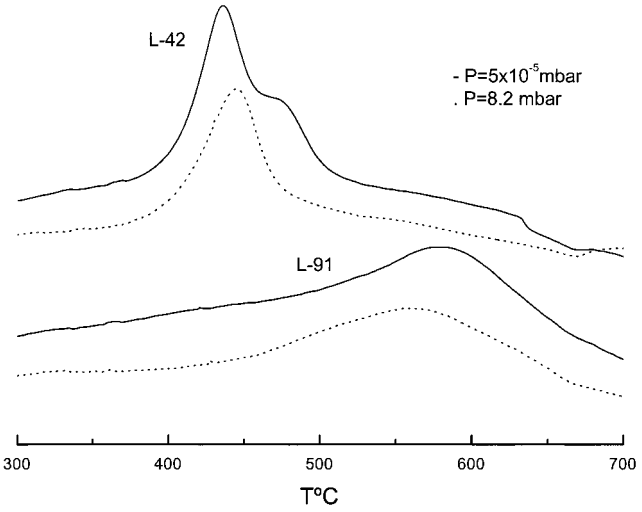

Figure 9. DSC curves recorded under dry helium flow for a series of iron oxides previously obtained from the thermal decomposition of the L-43 and L-92 lepidocrocite precursors under different constant values of the residual pressure of water vapor.

γ-Fe_2O_3 obtained from the L-92 precursor is much lower than those obtained for the phase transformation of the maghemite samples coming from the L-43 precursor. These results point out that the higher the excess of energy stored by γ-Fe_2O_3, with regard to the energy stored by the α-Fe_2O_3 resulting from the polymorphic conversion, the lower the thermal stability of the maghemite, according to the behavior that would be expected from thermodynamic considerations.

The results included in Figure 9 suggest that the thermal stability of maghemite does not seem to depend directly on its crystallite size, unless in the range from 4 to 10 nm here investigated. This conclusion is in disagreement with the statement of Vajpey et al.[47] which considered that the transition temperature increases by decreasing the crystal size of γ-Fe_2O_3 as estimated from specific surface measurements. It is worthy to note that the specific surface (82 $m^2\ g^{-1}$) measured for the maghemite obtained from the thermal decomposition of L-43 lepidocrocite under 5×10^{-5} mbar is not very different from the specific area (91 $m^2\ g^{-1}$) of the γ-Fe_2O_3 produced from the thermal decomposition of the L-92 lepidocrocite under a water vapor pressure equal to 8.2 mbar. However, the γ-$Fe_2O_3 \rightarrow \alpha$-$Fe_2O_3$ transition temperature reported for the latter sample is considerably higher than that of the former sample (Figure 9). In general, the maghemites samples coming from the L-92 precursor are much more stable than those obtained from the L-43 precursor. This behavior does not seem to be explained by the effect of the energy stored in the pores, because the temperatures of the phase transitions are identical for samples prepared from the same precursor but with different porosity. On the other hand, the precursor itself is an important parameter in the thermal stability of the maghemite sample. In the present case, the larger stability of the ex-L92 maghemite could be related to its special structure composed of aggregated needlelike subunits, where the particle boundaries could inhibit the ion mobility and enhance the maghemite stability.

On the other hand, the use of the CRTA method here outlined has demonstrated that the increase in the specific surface of lepidocrocite during its transformation to maghemite is nearly independent of its decomposition rate as shown in Figure 6. Hence, the influence of water vapor in the microporosity of the sample cannot be interpreted considering that the decomposition rate of lepidocrocite decreases by increasing the partial pressure of water vapor. The decrease of the porosity of γ-Fe_2O_3 by increasing the water vapor pressure would be interpreted considering that H_2O promotes the surface migration resulting in faster pore growth and pore elimination at the time that an increase of the γ-Fe_2O_3 crystal size takes place. This interpretation is closed to those proposed by Hirokawa et al.[62] for explaining the influence of the water vapor in the evolution of the porosity of hematite obtained from the thermal decomposition of goethite. A similar influence of water vapor in the decomposition of gibsite[52] and the sintering of MgO,[63] a zirconia phase transition,[64] have been previously proposed.

Conclusions

In summary, after taking into account the results concerning to the influence of the water vapor pressure used for decomposing the L-43 lepidocrocite sample on the texture and structure of the final products, we can conclude that the catalytic effect of water vapor favors the Fe^{2+} mobility. Hence, water vapor simultaneously promotes both the elimination of the porosity, the increase of the particle size, and the maghemite $\rightarrow$ hematite phase transition. The results obtained using the L-92 lepidocrocite precursor can be explained by taking into account that this sample is constituted by a bundle of very narrow needle-shaped crystals. Thus, it would be considered that the boundaries limiting the elongated crystals hinder the ion mobility. This interpretation would explain that the porosity of the γ-Fe_2O_3 obtained from this sample is considerably lower than the corresponding one obtained under similar conditions for the L-43 precursor, as shown in Figure 6. This figure points out that the relative increase of the specific surface, as a result of the porosity generated during the thermal decomposition of the L-92 lepidocrocite sample, is smaller than the corresponding one generated during the thermal decomposition of the L-43 precursor. This behavior would also explain that the promoter effect of water vapor on the crystal size growth of the ex-L-43 γ-Fe_2O_3 sample is higher than the one exerted on the maghemite coming from the L-92 lepidocrocite precursor. The lower ionic mobility of the γ-Fe_2O_3 obtained from the latter precursor would also explain its higher stability toward the polymorphic transformation into hematite. This would also explain that the catalytic effect of water vapor on the phase transition of the γ-Fe_2O_3 obtained from L-92 precursor is lower than that for the polymorphic conversion into hematite of the maghemite obtained from the thermal decomposition of the L-43 lepidocrocite sample.

CM981062F

(62) Hirokawa, S.; Naito, T.; Yamaguchi, T. *J. Colloid Interface Sci.* **1985**, *112*, 268.
(63) Varela, J. A.; Whitmore, O. J. *Mater. Sci. Monogr.* **1982**, *14*, 439.
(64) Kim, D. J.; Jung, H. J.; Jang, J. W.; Lee, H. L. *J. Am. Ceram. Soc.* **1998**, *81*, 2294.